Active vibration isolation performance of the bistable nonlinear electromagnetic actuator with the elastic boundary

Kai Yang[1], Weihao Tong[1], Liquan Lin[1], Yurchenko Danill[2], Junlei Wang[3,*]

[1]*School of Aerospace Engineering, Huazhong University of Science and Technology, Wuhan 430074, China.*

[2]*Institute of Mechanical, Process & Energy Engineering, Heriot-Watt University, Edinburgh EH14 4AS, UK*

[3]*School of Mechanical and Power Engineering, Zhengzhou University, Zhengzhou 450000, China.*

*Corresponding authors. Email: jlwang@zzu.edu.cn

Abstract

This paper thoroughly investigates the broadband active vibration isolation of a bistable nonlinear electromagnetic actuator with an elastic boundary (simply named EB-bistable actuator). A new feedback control law is proposed to control the actuator's input current, so as to significantly attenuate the broadband vibration transmissibility from the base excitation to the actuator mover (supporting the payload). The control law comprises the polynomial function of the mover's absolute velocity. The mathematical model of the EB-bistable actuator and its application for vibration isolation is derived and experimentally validated. Then, based on the verified model, the paper comprehensively investigates the EB-bistable actuator with the proposed control law, which validates the broadband active vibration isolation performance for different system's parameters. The input-to-state stability (ISS) of the control law for any non-negative control weights is proved, and thus it is a model-free control method. Results of one investigated case show that, the maximum vibration transmissibility can be attenuated by over 90%. The lower bound of the effective vibration isolation bandwidth (where the vibration transmissibility is smaller than 0 dB) is reduced by 19.69%, i.e. the bandwidth is significantly broadened. Moreover, the study proves the effectiveness of the active vibration isolation for the structural variation and initial condition change. Finally, the paper thoroughly discusses the influence of the control law parameters on the active vibration isolation performance. The parametric studies develop the useful guidelines of the active vibration isolation of the EB-bistable actuator.

Keywords: active vibration isolation; bistable nonlinearity; electromagnetic actuator; elastic boundary

1. Introduction

The electromagnetic actuator can transfer the input current into the actuation force through the electromagnetic induction principle, so as to achieve the fast response [1, 2] . Many industrial machines use electromagnetic actuators for vibration [3-7] and robot control [8-10]. The conventional electromagnetic actuator employs a linear spring to reset the actuator mover. However, the linear spring force is always opposite to the actuation direction when the actuator is controlled by a dynamic signal, and hence it hampers the actuation, degrading the actuation efficiency. To improve the actuation efficiency, the nonlinear structure can be used instead of linear spring as an effective solution.

Bistable nonlinear system draws great attention owing to its unique physical feature of the twin-well potential. The twin-well potential can lead to the large amplitude 'inter-well' response [11-15], which is beneficial to actuation efficiency improvement. It is discovered that the bistable nonlinear spring has a 'negative linear spring' effect between the two stable equilibrium positions due to the twin-well configuration [11, 14]. Thus, the negative-linear-spring force is in the same direction of the actuation, leading to the significantly acceleration of the actuator. Enlightened by the bistable nonlinear spring feature, various types of the bistable actuators were proposed, which validate the actuation efficiency improvement [16-20]. For example, to improve stroke performance of the crawling robot motion, Fang et al. [18] proposed a bistable piezoelectric vibration-driven locomotion system. Harne et al. [20] investigated the dynamics of a buckle-beam-like bistable structure, and found that the bistable structure can significantly enhance the vibration response which may be used for design of the bio-inspired flapping wing vehicle.

Inspired by the discoveries of the previous researches that additional dynamic coupling can enhance the vibration responses of the bistable structure [21-23], our research group recently proposed a new bistable electromagnetic actuator with the elastic boundary (simply named EB-bistable actuator) [24-26]. The EB-bistable actuator adds another linear spring and joint mass to form the elastic boundary (EB) at one end of the bistable nonlinear spring, and thus the bistable nonlinearity is dynamically changed during the actuation [24]. The results show that the EB significantly improves the bistable actuator's actuation efficiency when controlled by the dynamic current signals [24].

Although the previous research explored the open-loop dynamic feature of the EB-bistable actuator, the application of this actuator for the closed-loop control has not yet been investigated. Active vibration isolation is a typical closed-loop control of the electromagnetic actuator [3, 27-29]. In the active control, the vibration response of the actuator mover (supporting the payload) is acquired by a sensor and it is fed back to a controller. The controller runs a control law to calculate the input signal, which drives the electromagnetic actuator to produce the actuation, leading to vibration attenuation of the mover. To shed light on application of the favorable EB-bistable actuator, this study will

thoroughly investigate the active vibration isolation of the new actuator. The paper will present a model-free control law which is stable for any non-negative control weights, proving its stability and validating its effective vibration isolation performance for a broad frequency band. Through the numerical and experimental studies, the paper will demonstrate a new effective control methodology for the broadband active vibration isolation of the nonlinear electromagnetic actuator.

The rest of this work is organized as follows. Section 2 states the theory of the EB-bistable actuator in detail. Section 3 presents experimental validation to show the fidelity of the mathematical modeling. Section 4 shows active vibration isolation performance of the EB-bistable actuator using the feedback control law. To develop the insight of the nonlinear dynamic behaviors, Section 5 discusses the time history results, phase plots and FFT results of the EB-bistable actuator with and without control at a specific excitation frequency. Afterwards, Section 6 comprehensively discusses how the control parameters affect the active vibration isolation performance, which would present the useful guidelines. Section 7 summarizes the key findings of this study.

2. Theory of the active vibration isolation of the EB-bistable actuator

2.1 Problem statement

Fig. 1 shows the schematic of the active vibration isolation of the bistable electromagnetic actuator with the elastic boundary (EB-bistable actuator). The EB-bistable actuator's mover m_1 supports the payload, which needs vibration isolation from the base excitation z. The mover m_1 has coils and the linear track installs the permanent magnet. Owing to the electromagnetic principle, the coil current i can produce the actuation force $F = \theta i$ (θ is the electromagnetic coupling constant that is related to the coil length and magnetic field strength [30-32]), which drives the mover m_1 to vibrate. The bistable nonlinearity is realized by the oblique spring with stiffness k_1, where the spring original length L_1 is greater than the height d (which is the distance between the connection point of the oblique spring on the mover and the bottom of linear spring when the system is static). Therefore, the oblique spring will be compressed at the center line, which pushes the mover away from the center line, leading to two stable equilibria. The other vertically placed spring k_2 and the joint mass m_2 constitute the elastic boundary (EB) that can dynamically vary the bistable nonlinearity. The EB was proved to significantly enhance the actuation responses in the our previous work [24].

The active vibration isolation process is presented as follows. A sensor (accelerometer or laser vibrometer) is used to acquire the absolute vibration quantity (displacement, velocity or acceleration) of the payload. The measured vibration quantity is fed back to a controller which runs the control law algorithm to calculate the control signal. Afterwards, the control signal is linearly transformed into the coil current i with a power amplifier. The current i produces the electromagnetic force $F = \theta i$ to actively attenuate the payload vibration.

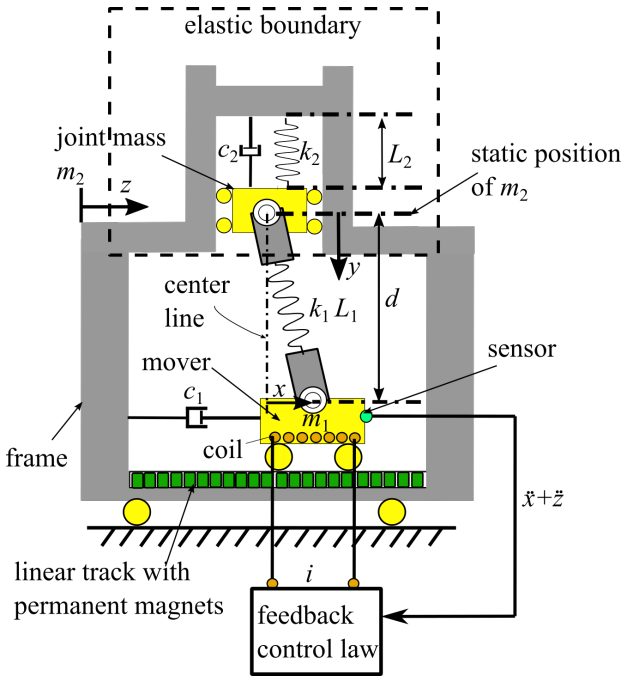

Fig. 1 The schematic of the bistable electromagnetic actuator with elastic boundary (EB-bistable actuator) for active vibration isolation. The vibration of the mover (supporting the payload) should be attenuated by controlling the current *i*, when the frame is subjected to the base vibration excitation.

2.2 Mathematical modeling

The kinetic, potential energy and dissipation functions are expressed as follows,

$$T_e = \frac{1}{2}m_1(\dot{x}+\dot{z})^2 + \frac{1}{2}m_2(\dot{y}^2+\dot{z}^2) \tag{1}$$

$$V_e = \frac{1}{2}k_1\left(\sqrt{(d-y)^2+x^2}-L_1\right)^2 - m_2gy + \frac{1}{2}k_2y^2 \tag{2}$$

$$D_e = \frac{1}{2}c_1\dot{x}^2 + \frac{1}{2}c_2\dot{y}^2 \tag{3}$$

where x is the displacement of the mover deviating from the center line, y is the displacement of the joint mass deviating from the static position, and z is the base excitation displacement, $\ddot{x}+\ddot{z}$ is the absolute vibration acceleration that needs to be attenuated for active vibration isolation, c_1 and c_2 are the linear damping induced by the track supporting m_1 and m_2, respectively.

Using the Lagrange's equations, the governing equations of the EB-bistable actuator subjected to the base excitation are

$$m_1(\ddot{x}+\ddot{z}) + \frac{k_1x}{\sqrt{(d-y)^2+x^2}}\left(\sqrt{(d-y)^2+x^2}-L_1\right) + c_1\dot{x} = \theta i \tag{4}$$

$$m_2\ddot{y} - m_2g + k_2y + \frac{k_1(y-d)}{\sqrt{(d-y)^2+x^2}}\left(\sqrt{(d-y)^2+x^2}-L_1\right) + c_2\dot{y} = 0 \tag{5}$$

where $F=\theta i$ is the electromagnetic force.

Defining the parameters in Table 1, the governing equations are simplified to be

$$\ddot{x} + 2\zeta_1\omega_1\dot{x} + \omega_1^2 x\left(1 - \frac{\alpha d}{\sqrt{x^2+(d-y)^2}}\right) = \frac{\theta}{m_1} i - \ddot{z} \tag{6}$$

$$\ddot{y} + 2\zeta_2\omega_2\dot{y} + \omega_2^2 y + \mu\omega_1^2(y-d)\left(1 - \frac{\alpha d}{\sqrt{x^2+(d-y)^2}}\right) - g = 0 \tag{7}$$

Note that the length ratio $\alpha = L_1/d > 1$, and thus there are two stable equilibria of the mover:$x_{eq} = \pm\sqrt{\alpha^2 d^2 - \left(d - \frac{g}{\omega_2^2}\right)^2}$, i.e. the system is bistable. It is seen that the vibration displacement y affects the system bistable nonlinear restoring force $\omega_1^2 x\left(1 - \frac{\alpha d}{\sqrt{x^2+(d-y)^2}}\right)$. That is, the elastic boundary can dynamically vary the bistable nonlinearity.

Table 1 Definition of the normalized parameters

Parameter	Expression
Mass ratio	$\mu = m_1/m_2$
Oblique spring natural frequency	$\omega_1 = \sqrt{k_1/m_1}$
Linear spring natural frequency	$\omega_2 = \sqrt{k_2/m_2}$
Mover damping ratio	$\zeta_1 = c_1/2m_1\omega_1$
Joint mass damping ratio	$\zeta_2 = c_2/2m_2\omega_2$
Length ratio	$\alpha = L_1/d$

The vibration isolation performance can be evaluated by using the vibration transmissibility from the excitation acceleration to the mover (which supports the payload) absolute acceleration,

$$T = \frac{Amp(\ddot{x}+\ddot{z})}{Amp(\ddot{z})} \tag{8}$$

where Amp represents the amplitude. That is, the smaller vibration transmissibility T indicates the better vibration isolation performance. Thus, the goal of the active vibration isolation is to find the appropriate control current i to attenuate the vibration transmissibility T.

3. Experimental validation

2.1 Experimental setup

Before discussion of the active vibration isolation using the EB-bistable actuator, the mathematical model of the actuator should be validated. Two experiments are performed to validate both the dynamic responses of the EB-bistable actuator under the swept harmonic current i and the open-loop responses of the actuator mounted on a shaker (where the input current $i = 0$). The experimental setup is shown in Fig. 2. Fig. 2 (a) shows the prototype of the EB-bistable actuator, and the approximate structural parameters of the prototype are presented in Table 2. The parameters in Table 2 are obtained as follows: the mover mass m_1 and the joint mass m_2 are measured using an electronic balance, spring stiffness k_1 and k_2 are obtained by measuring their static deformations when supporting a unit mass (1 Kg). Following the same method of Refs. [33, 34] in measuring the

electromagnetic interaction, the electromechanical coupling θ are calculated by both of the static input current i and the force of the actuator mover F (i.e. $\theta = F/i$). The static input current is produced by a direct current source, and force F is measured by a force sensor. The damping ratios ζ_1 and ζ_2 are estimated through parameter identification where only the linear vibration response has been activated using the small-strength excitation. Fig. 2 (b) and (c) show the schematics of the two experiments. In Fig. 2 (b), the EB-bistable actuator's frame is fixed on the ground and the swept harmonic current with rate 0.05 Hz/s is used to excite the actuator. The current i comes from an amplifier connecting a function generator, where voltage signal of 1 V produced by the function generator can be transformed into current of 0.42 A. An accelerometer is used to acquire absolute vibration acceleration of the mover. On the other hand, as shown in Fig. 2 (c), the EB-bistable actuator is mounted on a shaker, where the shaker produces the swept harmonic base excitation with rate 0.05 Hz/s. The experiment in Fig. 2 (b) can validate the mathematical model of the actuator under harmonic input current in a wide frequency band, whereas the experiment in Fig. 2 (c) can verify the dynamic response of the actuator subjected to the base excitation.

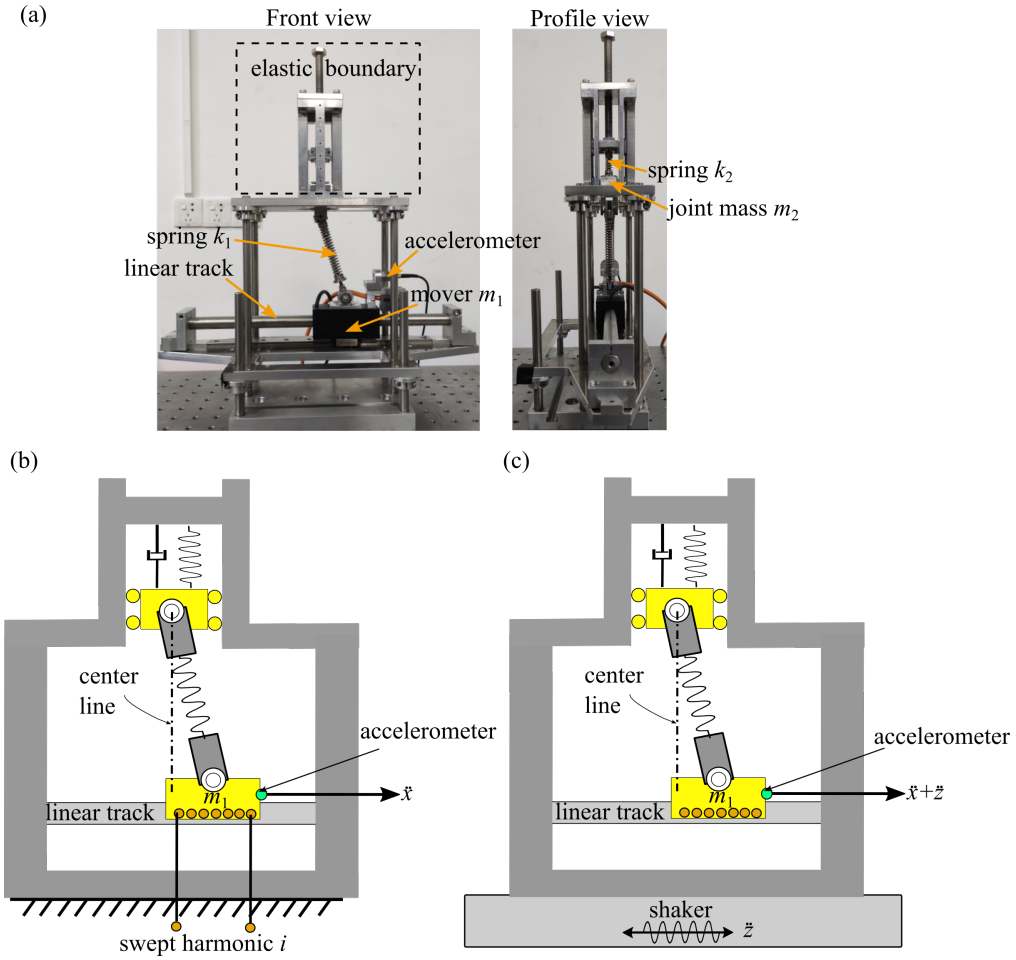

Fig. 2 (a) The prototype of the EB-bistable actuator, (b) experiment of the EB-bistable actuator under broadband input current, and (c) experiment of the EB-bistable actuator subjected to the broadband base excitation.

Table 2 Parameters of the experimental setup

Parameter	value
The mover mass m_1	0.578 kg
The joint mass m_2	0.031 kg
The oblique spring stiffness k_1	2940 N/m
The elastic boundary spring stiffness k_2	980 N/m
The damping ratio ζ_1	0.015
The joint mass damping ratio ζ_2	0.0008
The oblique spring length L_1	0.08 m
The height d	0.072 m
The electromagnetic coupling constant θ	9.3 N/A
The gravity acceleration g	9.8 N/m/s^2

2.2 Results

Fig. 3 shows the experimental and numerical results of the mover acceleration envelope of the EB-bistable actuator under the swept harmonic input current i with three different amplitudes [0.168, 0.189, 0.210] A (i.e. the function generator outputs are [0.40, 0.45, 0.50] V) in 0.1~12 Hz. Both the results of the actuator under the forward and backward swept currents are presented. Results show that for all the three amplitudes, the numerical results and experimental results are in good agreement in terms of the nonlinear dynamic behaviors despite of some value discrepancies at some frequencies. This validates the EB-bistable actuator model under the control current. It is also seen that the forward swept current can easily activate the large-amplitude vibration responses in the low frequency band.

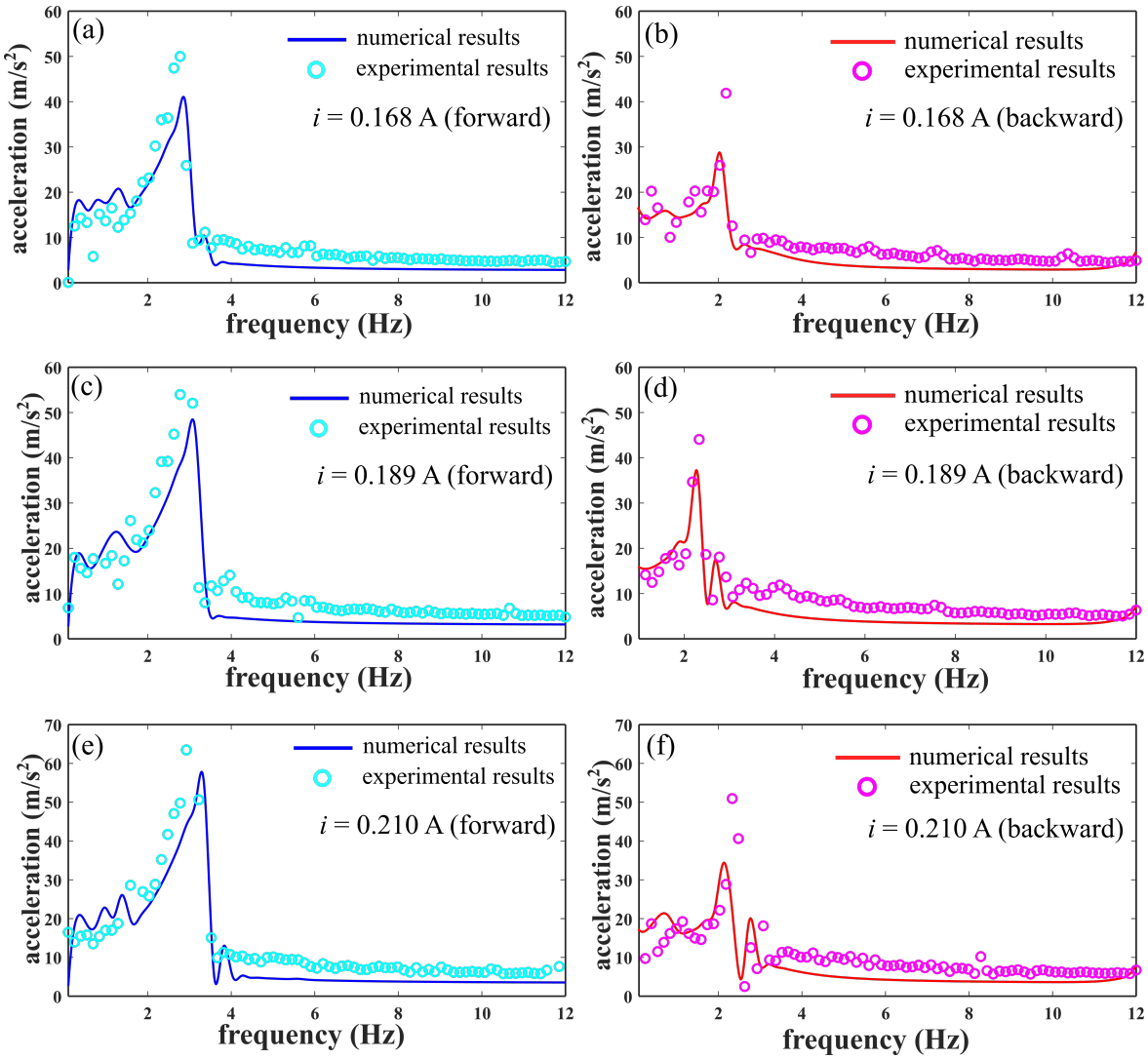

Fig. 3 The experimental and numerical results of the mover acceleration envelope of the EB-bistable actuator under (a)(c)(e) the forward swept harmonic input currents: (a) $i = 0.168$ A, (c) $i = 0.189$ A and (e) $i = 0.21$ A; (b)(d)(f) the backward swept harmonic input currents: (b) $i = 0.168$ A, (d) $i = 0.189$ A and (f) $i = 0.21$ A (i.e. the function generator outputs are [0.4, 0.45, 0.5] V)

Fig. 4 shows the experimental and numerical results of the mover absolute acceleration envelope of the EB-bistable actuator subjected to the base vibration excitations $\ddot{z}$ with three different amplitudes [2.07, 2.64, 2.94] m/s^2. The numerical predictions agree well with the experimental results for the three cases, which validates the open-loop performance of the EB-bistable actuator subjected to the base excitation, despite of some value discrepancies at some frequencies. The results show that the EB-bistable actuator would exhibit large vibration in the low frequency band (below 4 Hz), which would be attenuated via the active vibration isolation with an appropriate control law.

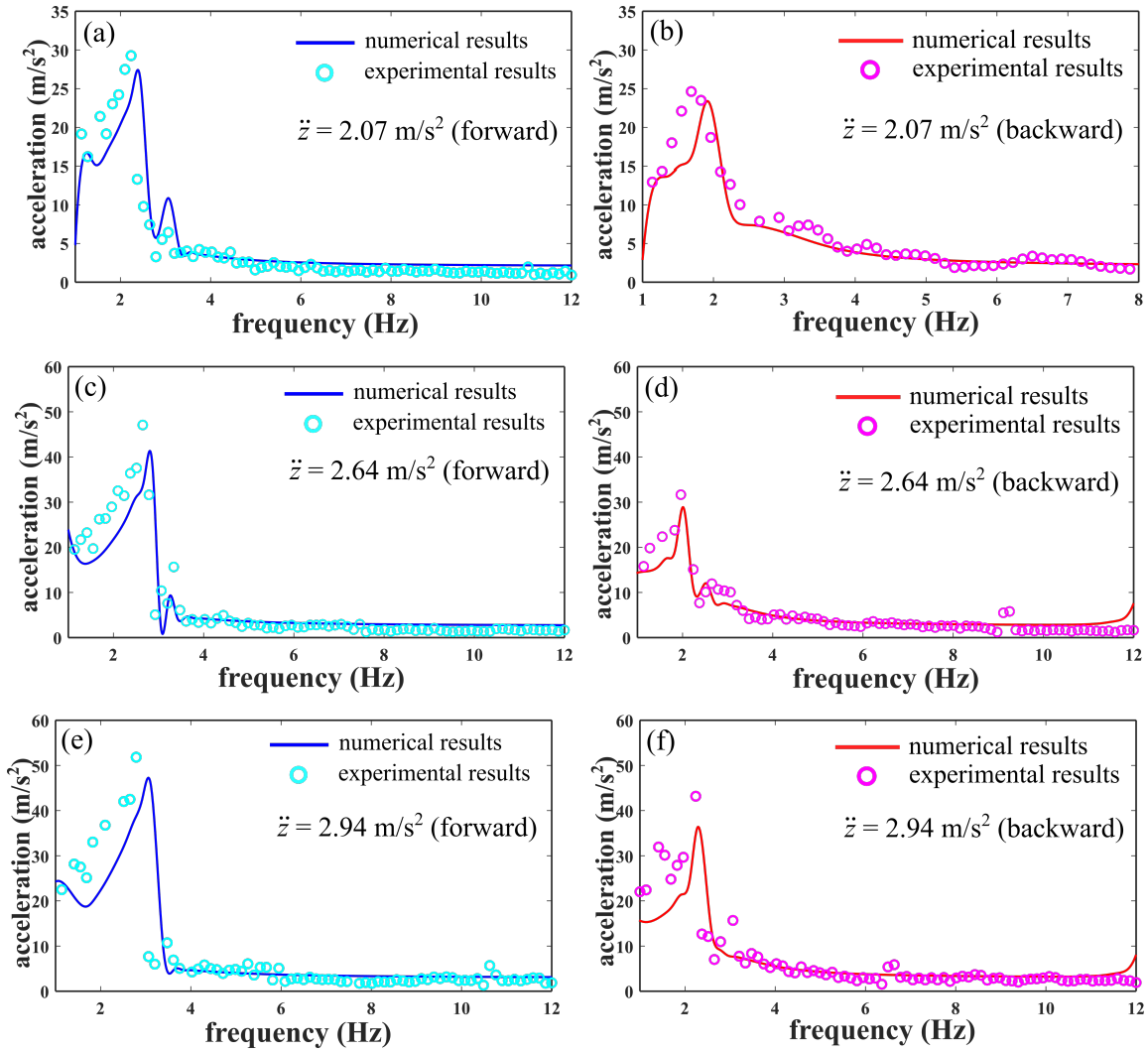

Fig. 4 The experimental and numerical results of the mover absolute acceleration envelope of the EB-bistable actuator subjected to (a)(c)(e) the forward swept base vibrations: (a) $\ddot{z} = 2.07$ m/s^2, (c) $\ddot{z} = 2.64$ m/s^2 and (e) $\ddot{z} = 2.94$ m/s^2; (b)(d)(f) the backward swept base vibrations: (b) $\ddot{z} = 2.07$ m/s^2, (d) $\ddot{z} = 2.64$ A and (f) $\ddot{z} = 2.94$ m/s^2

4. Active vibration isolation performance

4.1 The feedback control law

To attenuate the large vibration in the low frequency band discovered in the experiments, the following feedback control law for i is proposed,

$$i = -\frac{am_1}{\theta} v - \frac{bm_1}{\theta} v^3 \tag{9}$$

$$v = \int_0^t \ddot{x}(\tau) + \ddot{z}(\tau)\, \mathrm{d}\tau = \dot{x} + \dot{z} \tag{10}$$

where the linear-term and cubic-term control weights are a and b, respectively. Eq. (10) means that v is the integration of the ~~absolute~~ acceleration of the mover m_1, i.e. the ~~absolute~~ velocity. Note that, in practice, integration process of $\ddot{x}(\tau) + \ddot{z}(\tau)$ will induce a constant bias. This constant bias can be eliminated by using a capacitor at the frontend of the controller. $\ddot{x} + \ddot{z}$ can be obtained by an

accelerometer mounted on the mover, and the absolute velocity $\dot{x}+\dot{z}$ can be obtained by a Doppler laser velocimeter.

Therefore, the closed-loop control equations of the system become

$$\ddot{x}+2\zeta_1\omega_1\dot{x}+\omega_1^2 x\left(1-\frac{\alpha d}{\sqrt{x^2+(d-y)^2}}\right)=-av-bv^3-\ddot{z} \tag{11}$$

$$\ddot{y}+2\zeta_2\omega_2\dot{y}+\omega_2^2 y+\mu\omega_1^2(y-d)\left(1-\frac{\alpha d}{\sqrt{x^2+(d-y)^2}}\right)-g=0 \tag{12}$$

It is seen that the control weights a and b affect the vibration transmissibility T, and their values range to keep the control stability, will be presented in next subsection.

4.2 The input-to-state stability

Before discussing the active vibration isolation performance, the stability of the proposed control law should be investigated. For Eqs. (10)--(12), $\ddot{z}$ (the external base excitation) can be treated as the system input, and thus input-to-state stability (ISS) [35] of the controlled system is selected to search the appropriate control weights a and b. Note that, $\ddot{z}$ is the external harmonic vibration excitation which is a bounded signal. That is, $u_1=\ddot{z}$, $u_2=\dot{z}$ are the external inputs of the closed-loop system (Eqs. (10)--(12)).

Let $[q_1,q_2,q_3,q_4]=[x,\dot{x},y-y_{st},\dot{y}]$, where $y_{st}=g/\omega_2^2$. Eqs. (10)--(12) can be rewritten as

$$\dot{q}_1=q_2 \tag{13}$$

$$\dot{q}_2=-2\zeta_1\omega_1 q_2-\omega_1^2 q_1\left(1-\frac{\alpha d}{\sqrt{q_1+(q_3+y_{st}-d)^2}}\right)-av-bv^3-u_1 \tag{14}$$

$$\dot{q}_3=q_4 \tag{15}$$

$$\dot{q}_4=-2\zeta_2\omega_2 q_4-\omega_2^2 q_3-\mu\omega_1^2(q_3+y_{st}-d)\left(1-\frac{\alpha d}{\sqrt{{q_1}^2+(q_3+y_{st}-d)^2}}\right) \tag{16}$$

$$v=q_2+u_2 \tag{17}$$

Define the following smooth function

$$V_L=\frac{1}{2}q_2^2+\frac{1}{2\mu}q_4^2+\frac{1}{2}\omega_1^2\left(\sqrt{q_1^2+(q_3+y_{st}-d)^2}-\alpha d\right)^2+\frac{1}{2\mu}\omega_2^2 q_3^2 \tag{18}$$

V_L is positive-definite due to $\mu>0$. Therefore, there are $K\infty$ functions $\alpha_1(|q_2|)=\frac{1}{2}|q_2|^2$ and $\alpha_2(|q_2|)=2V_L$, which satisfy

$$\alpha_1(|q_2|)\le V_L\le\alpha_2(|q_2|) \tag{19}$$

The derivative of V_L with respect to time *t* is

$$\begin{aligned}\dot{V}_L=&\,q_2\dot{q}_2+q_2\omega_1^2 q_1\left(1-\frac{\alpha d}{\sqrt{q_1+(q_3+y_{st}-d)^2}}\right)+\frac{1}{\mu}q_4\dot{q}_4\\&+q_4\omega_1^2(q_3+y_{st}-d)\left(1-\frac{\alpha d}{\sqrt{{q_1}^2+(q_3+y_{st}-d)^2}}\right)^2+\frac{1}{\mu}q_4\omega_2^2 q_3\end{aligned} \tag{20}$$

That is,

$$\dot{V}_L=-2\zeta_1\omega_1 q_2^2-\frac{2}{\mu}\zeta_2\omega_2 q_4^2-a(q_2+u_2)q_2-b(q_2+u_2)^3 q_2-u_1 q_2 \tag{21}$$

Since $u_1 = \ddot{z}$ is a harmonic excitation with an amplitude A, $u_2 = \dot{z}$ is also a harmonic excitation with an amplitude A/ω, where ω is the angular frequency of the excitation. This means that $|u_1| \leq A$ and $\omega|u_2| \leq A$.

When

$$|q_2| \geq \max\left(\frac{1}{\epsilon}|u_1|, \frac{\omega}{\epsilon}|u_2|\right) \tag{22}$$

i.e. $|q_2| \geq \frac{1}{\epsilon}|u_1|$ and $|q_2| \geq \frac{\omega}{\epsilon}|u_2|$, where ϵ is a small positive quantity, it is seen that

$$(q_2 + u_2)q_2 \geq q_2^2 - \frac{\epsilon}{\omega}q_2^2 = \left(1 - \frac{\epsilon}{\omega}\right)|q_2|^2 \tag{23}$$

$$(q_2 + u_2)^3 q_2 \geq \left(q_2 - \frac{\epsilon}{\omega}q_2\right)^3 q_2 = \left(1 - \frac{\epsilon}{\omega}\right)^3 |q_2|^4 \tag{24}$$

$$u_1 q_2 \geq -\epsilon|q_2|^2 \tag{25}$$

Therefore,

$$\dot{V}_L \leq -2\zeta_1\omega_1|q_2|^2 - \frac{2}{\mu}\zeta_2\omega_2|q_4|^2 - a\left(1 - \frac{\epsilon}{\omega}\right)^3 |q_2|^4 - b\left(1 - \frac{\epsilon}{\omega}\right)^3 |q_2|^4 + \epsilon|q_2|^2 \tag{26}$$

when the vibration frequency $\omega > \epsilon$ and $\epsilon \leq 2\zeta_1\omega_1$, for any control weights $a \geq 0$ and $b \geq 0$, the following inequality can be obtained,

$$\dot{V}_L \leq -\alpha(|q_2|) \tag{27}$$

where

$$\alpha(|q_2|) = a\left(1 - \frac{\epsilon}{\omega}\right)^3 |q_2|^4 + b\left(1 - \frac{\epsilon}{\omega}\right)^3 |q_2|^4 + \frac{2}{\mu}\zeta_2\omega_2|q_4|^2 \tag{28}$$

It is seen that $\alpha(|q_2|)$ is positive-definite. Therefore, the smooth function V_L is an ISS Lyapunov function. According to the Lemma 2.10 in Ref. [35], the control system (Eqs. (10)-(12), i.e. Eqs. (13)-(16)) is stable for any control weights $a \geq 0$ and $b \geq 0$, under the condition where the vibration frequency $\omega > \epsilon$ and $\epsilon \leq 2\zeta_1\omega_1$. It is noted that since ϵ is a very small quantity, condition $\omega > \epsilon$ represents a broad frequency band, and the condition $\epsilon \leq 2\zeta_1\omega_1$ can be easily satisfied for a real actuator. On the other hand, when assuming the inputs $u_1 \equiv 0$ (i.e., $u_2 \equiv 0$), Eq.(21) show that $\dot{V}_L$ is negative-definite, and therefore V_L is a "classic" Lyapunov function for $a \geq 0$ and $b \geq 0$. Overall, for the active vibration isolation of the EB-bistable actuator, the control weights $a \geq 0$ and $b \geq 0$ can ensure the stability of the control system.

4.3 The effectiveness of the active vibration isolation

Assume $\ddot{z} = -A\sin\Omega t$, where A is the excitation amplitude and Ω is the excitation frequency. The control simulation is performed in Matlab-Simulink, where the numerical integration uses the 4th Runge-Kutta method with 0.001 s time interval. The values of the structural parameters are presented in Table 3, they are close to the parameters of the prototype in Fig. 2. The initial conditions are $[x_0, \dot{x}_0, y_0, \dot{y}_0] = [-0.0353,\ 0,\ 0,\ 0]$, where $x_0 = -0.0353$ is the negative stable equilibrium of the actuator. As shown in Fig. 3 and 4, the forward swept excitation can easily activate the large-amplitude

vibration response in the low frequency band (which needs vibration isolation). Thus, in the following results, only the results subjected to the forward swept excitation are presented. The excitation frequency Ω is linearly increased in the forward sweeping with the rate 0.05 Hz/s.

Table 3 Values of the parameters for simulation

Parameter	value
Mass ratio μ	18
Oblique spring natural frequency ω_1	70 rad/s
Linear spring natural frequency ω_2	180 rad/s
Mover damping ratio ζ_1	0.015
Joint mass damping ratio ζ_2	0.0008
Length ratio α	1.11
Height d	0.072
Electromagnetic coupling for unit mass θ/m_1	16

Fig. 5 (a)-(c) show the vibration transmissibility results T of the EB-bistable actuator with and without active control subjected to three different excitation strengths $A = [1.5, 3, 6]$ m/s^2. For the EB-bistable actuator without control, different excitation strengths can lead to distinct vibration responses. The larger excitation strengths can significantly broaden the bandwidth of the high-orbit response and improve the amplitude of the vibration transmissibility T. As shown in Fig. 5 (b)-(c), when the excitation frequency Ω is greater than a value, (e.g. $\Omega >$ 6.45 Hz for A = 6 m/s^2 in Fig. 5 (c)), the saddle-node (SN) bifurcation occurs where the high-orbit vibration response (inter-well response) suddenly becomes the small-amplitude vibration response (intra-well response). It is noted that while increasing the mover damping ratio ζ_1 by four times (i.e. $\zeta_1 = 0.06$) can significantly attenuate the high-orbit vibration, the larger damping ratio saliently deteriorates the vibration isolation performance in the higher frequency band. That is, the vibration transmissibility in the higher frequency band is increased. Thus, for the effective broadband vibration isolation, active control method is introduced to attenuate the high-orbit vibration in the lower frequency band and retain the vibration isolation performance in the higher frequency band.

For the smaller damping ratio case ($\zeta_1 = 0.015$), when the control coefficients $a = 3$ and $b = 3$, the vibration transmissibility in the high-orbit vibration response are significantly degraded for all the three excitation strengths, whereas the high-frequency vibration transmissibility is same as in the case without control. That is, the active vibration isolation can not only significantly degrade the broadband vibration in the low frequency band, but also keep the effective vibration isolation performance in the higher frequency band. For example, as shown in Fig. 5(c), when the active control is off, two significant high-orbit vibration responses are excited due to the strongly nonlinearity, where the maximum transmissibility T are 27.00 dB and 11.42 dB for the first and second high-orbit responses,

respectively. At the same frequency locations, the transmissibility of the EB-bistable actuator with the active control are 2.44 dB and -12.10 dB. That is, the vibrations are attenuated by 24.56 dB and 23.52 dB, respectively, leading to the effective vibration isolation by over 90% (20 dB attenuation = 90% attenuation). It is also seen that in the higher frequency band, the vibration transmissibility curve of the EB-bistable actuator with control coincides with the curve without control for $\zeta_1 = 0.015$. Hence, the high-frequency vibration isolation performance is retained.

Defining the effective vibration isolation bandwidth is the frequency band where the vibration transmissibility $T < 0$ dB. As shown in Fig. 5 (c), the effective vibration isolation bandwidth without control is $\Omega > 6.45$ Hz, whereas the effective vibration isolation bandwidth with control becomes $\Omega > 5.18$ Hz. That is, the lower bound of the effective vibration isolation bandwidth is reduced by 19.69% ((6.45-5.18) / 6.45). Moreover, the control current i are smaller than 0.06, 0.23 and 0.71 A for $A = [1.5, 3, 6]$ m/s^2, respectively, which indicates that the needed control power is small and is easy to be realized in practical application. Overall, the results prove the broadband vibration isolation of the feedback control.

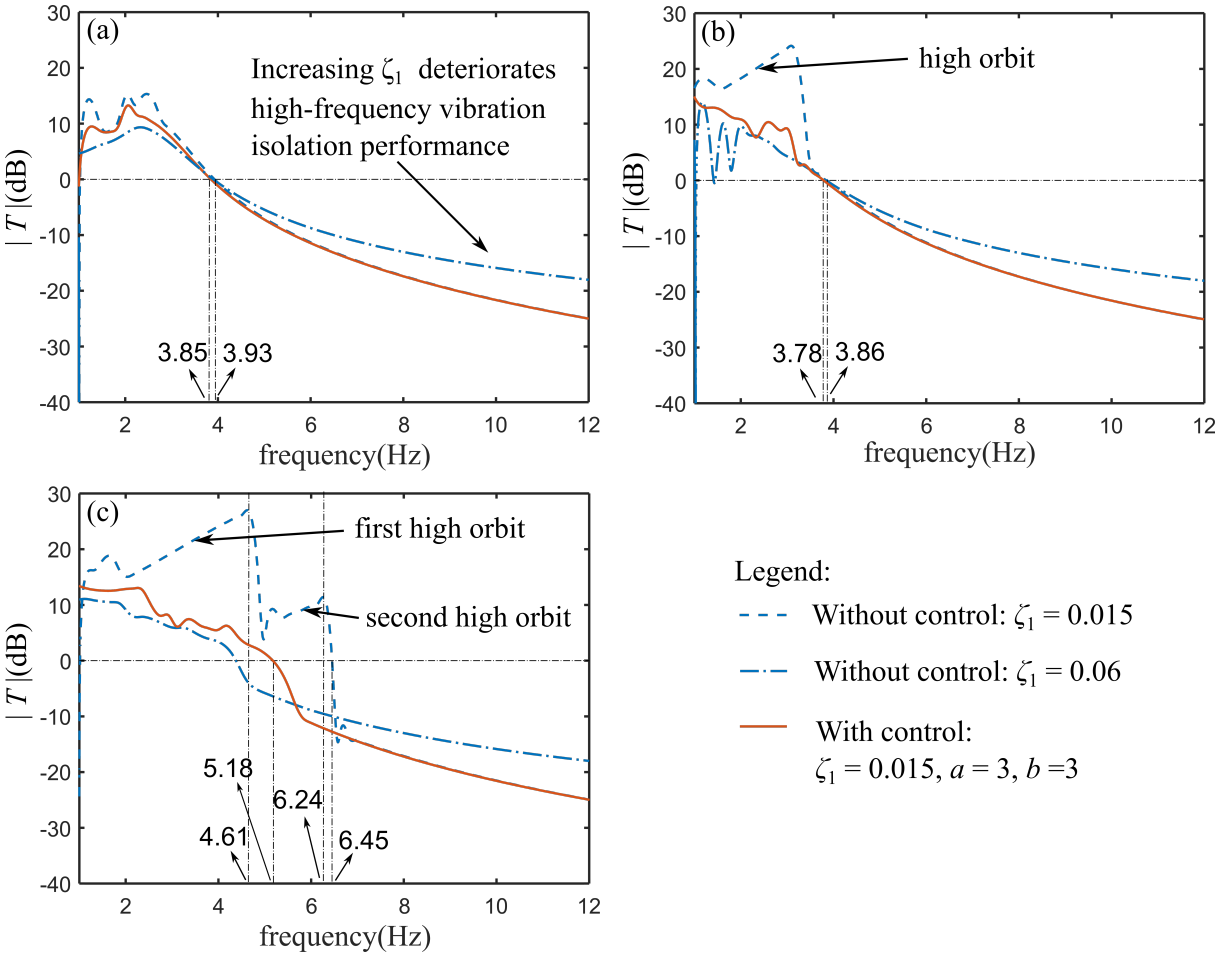

Fig. 5 vibration transmissibility results T of the EB-bistable actuator with and without active control subjected to four different excitation strengths $A = [1.5, 3, 6]$ m/s^2 : (a) $A = 1.5$ m/s^2, (b) $A = 3$ m/s^2 and (c) $A = 6$ m/s^2

Taking $A = 3$ m/s^2 as the example, the following results are presented to prove the effectiveness

robustness of the active vibration isolation. Fig. 6 (a)-(d) show the vibration transmissibility results T of the EB-bistable actuator with and without active control with respect to four different linear spring natural frequencies $\omega_2 = [50\ 70\ 180\ 240]$ rad/s, where $\omega_1 = 70$ rad/s. In this figure, $\zeta_1 = 0.015$. Results show that different ω_2 lead to significant variations of vibration transmissibility of the EB-bistable actuator without control, where the amplitudes and frequency ranges of the high-orbit responses are different. When the active control is used, for each of the four cases, the vibration transmissibility in the high-orbit response area is significantly attenuated and the high-frequency vibration isolation is also retained. That is, the active vibration isolation is effective for each of the four cases. This indicates that the active vibration isolation is strongly robust against the significant structural variations.

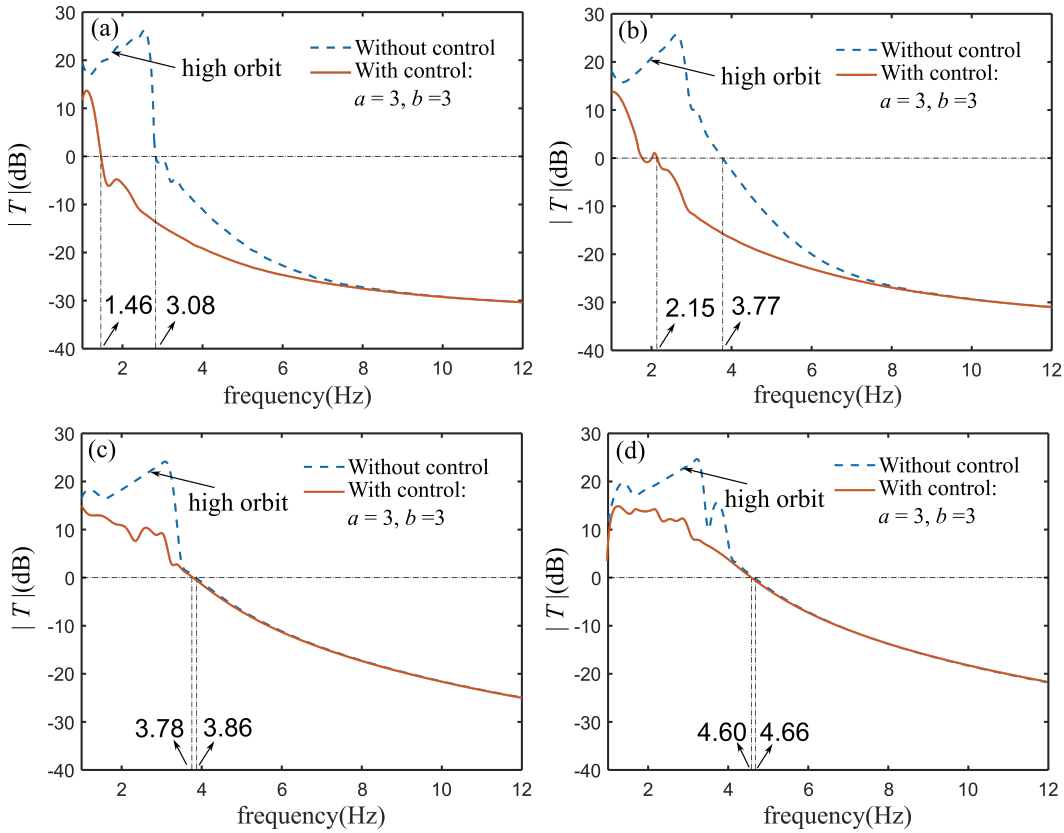

Fig. 6 Vibration transmissibility results T of the EB-bistable actuator with and without active control subjected to four different linear spring natural frequencies $\omega_2 = [50\ 70\ 180\ 240]$ rad/s, where $A = 3$ m/s^2, $\omega_1 = 70$ rad/s, $\zeta_1 = 0.015$: (a) $\omega_2 = 50$ rad/s, (b) $\omega_2 = 70$ rad/s, (c) $\omega_2 = 180$ rad/s and (d) $\omega_2 = 240$ rad/s.

5. The nonlinear dynamic behaviors

To develop the insight of the nonlinear dynamic behaviors of the EB-bistable actuator in active vibration isolation, the responses at the specific frequency 4.61 Hz (maximum T in the first high orbit) for $\zeta_1 = 0.015$ in Fig. 5(c) are investigated. Note that, different initial conditions may lead to distinct types of dynamic behaviors (e.g. single-periodic oscillation, chaos, etc.). Therefore, at the frequency 4.61 Hz, the study uses the random initial conditions to activate the distinct dynamic

behaviors, and the typical dynamic behaviors are presented as follows.

Fig. 7 shows the time history results, the phase plots and the FFT results at 4.61 Hz, where the initial conditions are $[x_0, \dot{x}_0, y_0, \dot{y}_0] = [-0.1422,\ -0.1774,\ 0.0488,\ -0.1961]$. The results show that when the EB-bistable actuator is not controlled, the periodic inter-well response due to the bistable nonlinearity is excited, where there is a single loop in the phase plot and a dominant spectrum line at 4.61 Hz. For this periodic response, the mover jumps between both the stable equilibria and its absolute acceleration amplitude is very large (nearly 129.12 m/s^2). With help of the active control, the vibration acceleration amplitude of the mover is decreased by over 90%, leading to significant vibration isolation. Interestingly, the dynamic behavior of the mover is changed into multi-periodic intra-well response, where the phase plot shows that the mover is oscillating around one of the stable equilibria following multiple loops. As shown in Eq. (11), the normalized control force $-av - bv^3$ emulates a virtual damper that connects the mover and the ground, and thus it consumes the vibration energy. As a result, the base excitation can no longer activate the large-amplitude inter-well vibration at the given frequency.

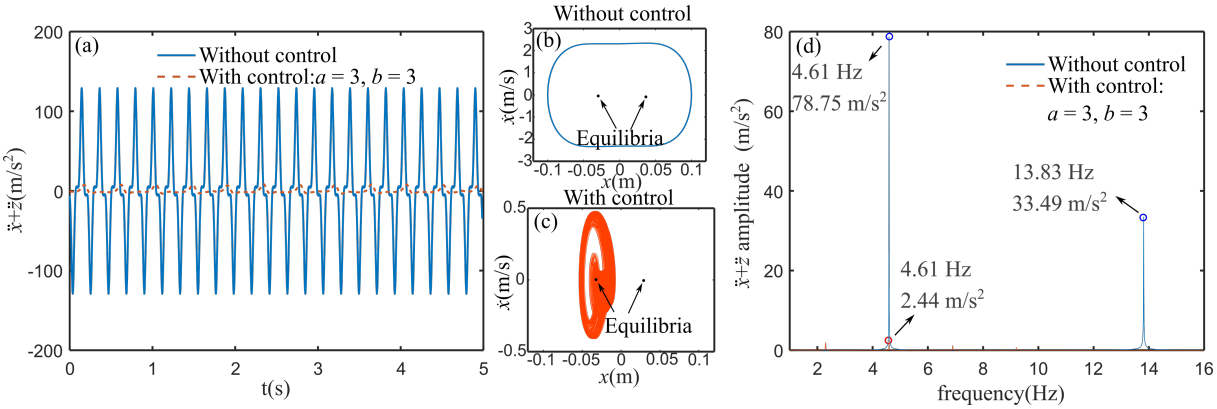

Fig. 7 (a) The time history results, (b) (c) the phase plots and (d) the FFT results of the EB-bistable actuator with and without control at 4.61 Hz, where the initial conditions are $[x_0, \dot{x}_0, y_0, \dot{y}_0] = [-0.1422,\ -0.1774,\ 0.0488,\ -0.1961]$.

Fig. 8 shows the time history results, the phase plots and the FFT results at 4.61 Hz for the initial conditions $[x_0, \dot{x}_0, y_0, \dot{y}_0] = [-0.0353,\ 0,\ 0,\ 0]$, where $x_0 = -0.0353$ is the negative stable equilibrium of the actuator. It is seen that the EB-bistable actuator without control exhibits the chaotic inter-well responses and the maximum vibration acceleration amplitude becomes 18.00 m/s^2. However, for this initial condition, the EB-bistable actuator with control exhibits the same multi-periodic intra-well response as Fig. 7, where there are subharmonic (1/2 periodic: 2.31 Hz), fundamental periodic (4.61 Hz), and superharmonic (e.g. 3/2 periodic: 6.92 Hz) components. The maximum amplitude of the absolute vibration acceleration under control is 8.37 m/s^2, and thus 53.50% vibration isolation is achieved. This indicates that the active vibration isolation is robust against the variation of the initial conditions.

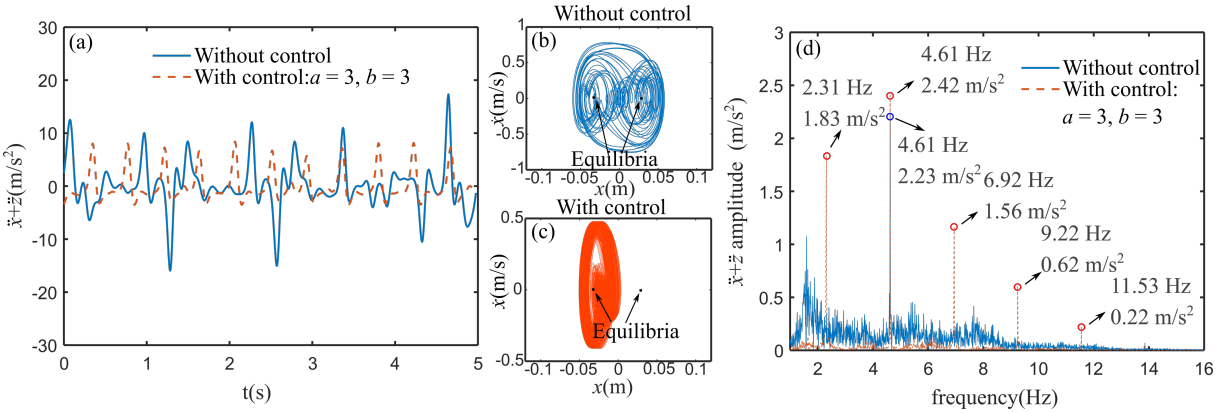

Fig. 8 (a) The time history results, (b) (c) the phase plots and (d) the FFT results of the EB-bistable actuator with and without control at 4.61 Hz, where the initial conditions are $[x_0, \dot{x}_0, y_0, \dot{y}_0] = [-0.0353, 0, 0, 0]$, where $x_0 = -0.0353$ is the negative stable equilibrium.

6. Performance study of the control parameters

To present the guidelines of the active control of the EB-bistable actuator, the following parametric studies are performed to discuss how the control weights a and b influence the active vibration isolation performance of the EB-bistable actuator. The initial values of the structural parameters are presented in Table 3 and the case where moderate excitation strength $A = 3$ m/s^2 and $A = 6$ m/s^2 are investigated as examples. The initial conditions are $[x_0, \dot{x}_0, y_0, \dot{y}_0] = [-0.0353,\ 0,\ 0,\ 0]$.

6.1 For moderate excitation strength $A = 3$

Fig. 9 (a) and (b) show the vibration transmissibility variation of the EB-bistable actuator with different combinations of the control weights. The vibration transmissibility of the EB-bistable actuator without control is also presented as the benchmark. Fig. 9 (a) discusses how the active vibration isolation is influenced by the following control parameters: $a = 1, 3, 5$ and $b = 0$ (i.e. only the linear term of the control current is kept). Results show that the active control attenuates the vibration transmissibility between the frequency 1.15 Hz and 3.43 Hz for $a = 1$ in the high orbit. However, the vibration isolation performance is deteriorated between 3.43 Hz to 3.82 Hz. When a is raised to $a = 3$, the effective vibration isolation bandwidth is significantly broadened, and the vibration transmissibility is saliently degraded. By increasing the linear term control weight a to be $a = 5$, the vibration isolation performance is further enhanced compared to the case $a = 3$. Hence, for $b = 0$, increasing the linear-term control weight a is beneficial to the active vibration isolation.

As shown in Fig. 9 (b), when $a = 1$ and $b = 3$, the active control attenuates the vibration transmissibility from 1.12 Hz to 3.51 Hz compared to the case $a = 1$ and $b = 0$ in Fig. 9 (a). For the case $a = 3$ and $b = 3$, the increased linear-term weight a is more beneficial to the vibration isolation. When a continues to increase, the vibration isolation performance is slightly enhanced. Comparing Fig. 9 (a) and (b), it is seen that the linear-term weight a is more effective than the cubic-term weight b for active vibration isolation. Therefore, adding b is beneficial to active

vibration isolation in the high-orbit response area when a is small and this cubic-term weight may be ineffective for vibration isolation for the larger linear-term control weight.

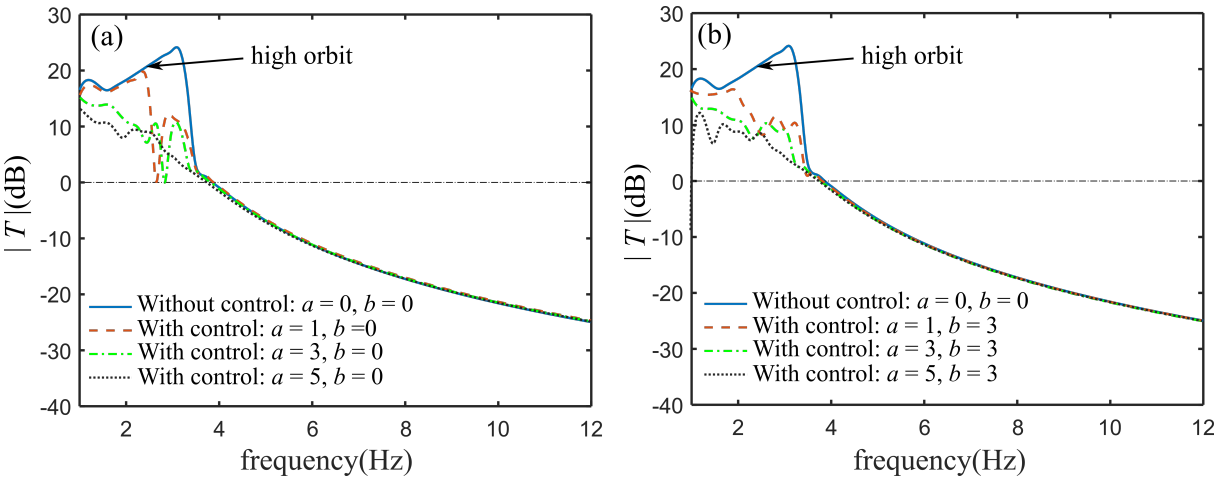

Fig. 9 Vibration transmissibility results of the EB-bistable actuator without and with active control for different control weights for $A = 3$ m/s^2: (a) $a = 1, 3, 5,\ b = 0$ (b) $a = 1, 3, 5,\ b = 3$

Fig. 10 (a) and (b) show the vibration transmissibility variation of the EB-bistable actuator with combinations of the control weights $a = 0, b = 1, 2, 3$ and $a = 3, b = 1, 2, 3$, respectively. As shown in Fig. 10 (a), when $a = 0$ (i.e. only the cubic-term control weight is kept), the vibration transmissibility can be lowered by increasing the cubic-term control weight b in the high-orbit frequency band by comparing $b = 1$ and $b = 3$. However, when $b > 3$, increasing b can only slightly enhance the active vibration isolation performance. As shown in Fig. 10 (b), when $a = 3$, changing b does not significantly vary the system vibration isolation performance. The results indicate that only when the linear-term control weight a is very small, increasing b is effective to active vibration isolation improvement.

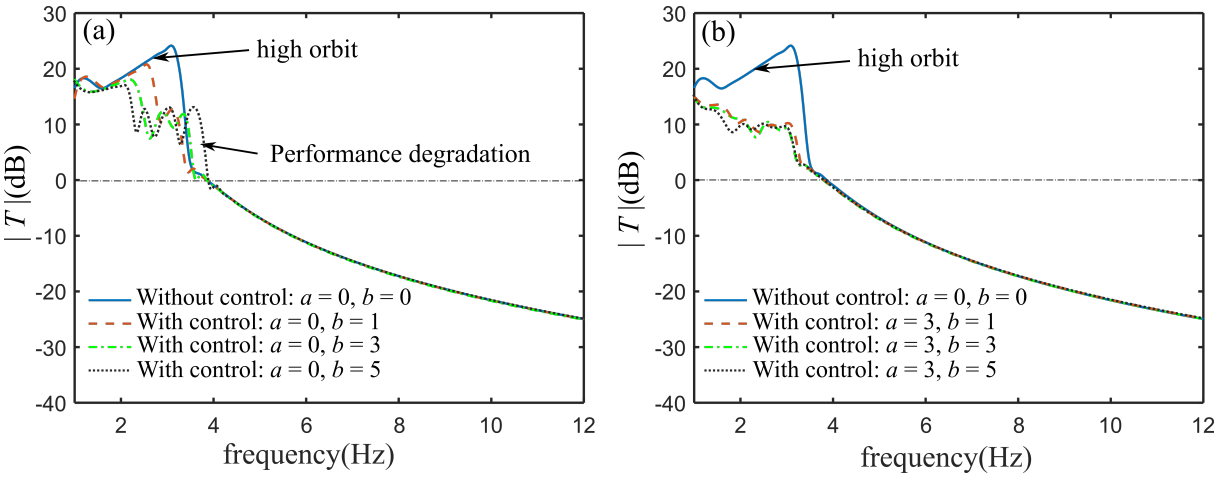

Fig. 10 Vibration transmissibility results of the EB-bistable actuator without and with active control subjected to different control weights for $A = 3$ m/s^2: (a) $a = 0,\ b = 1, 3, 5$ (b) $a = 3,\ b = 1, 3, 5$

6.2 For large excitation strength $A = 6$

The following studies uncover the variation trends of the active vibration isolation performance for

the large excitation strength $A = 6$ m/s^2. Fig. 11 shows the vibration transmissibility variation of the EB-bistable actuator with combinations of the control weights $a = 1,\ 2,\ 3,\ b = 0$ and $a = 1,\ 2,\ 3,\ b = 3$. It is seen that for both $b = 0$ and $b = 3$, increasing a can achieve better vibration isolation performance in the first and second high-orbit response area. Similar to the results in Fig. 9, when a is small, increasing the cubic-term control weight would be favorable to the active vibration isolation in the high-orbit response area.

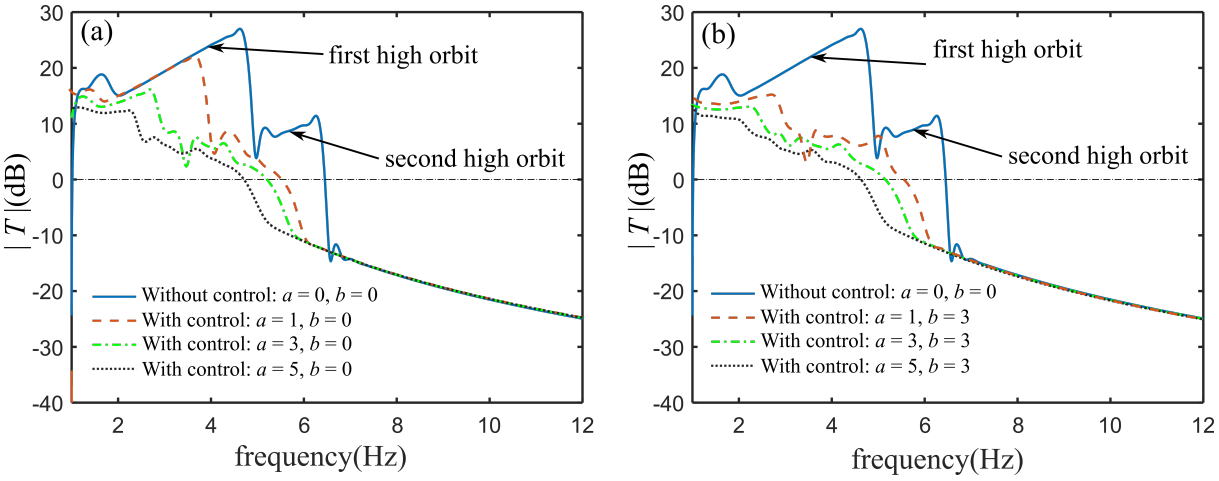

Fig. 11 Vibration transmissibility results of the EB-bistable actuator without and with active control for different control weights for $A = 6$ m/s^2: (a) $a = 1, 3, 5,\ b = 0$ (b) $a = 1, 3, 5,\ b = 3$

Fig. 12 shows the vibration transmissibility variation of the EB-bistable actuator with combinations of the control weights $a = 0, b = 1, 2, 3$ and $a = 3,\ b = 1, 2, 3$. It is seen that the variation trends of the active vibration isolation is also similar to the results in Fig. 10. That is, increased b is beneficial to the active vibration isolation when $a = 0$, whereas the vibration isolation performance slightly changed with respect to b when $a = 3$. This indicates that for large base excitation, the linear-term control weight affects the active vibration isolation more significantly than the cubic-term control weight.

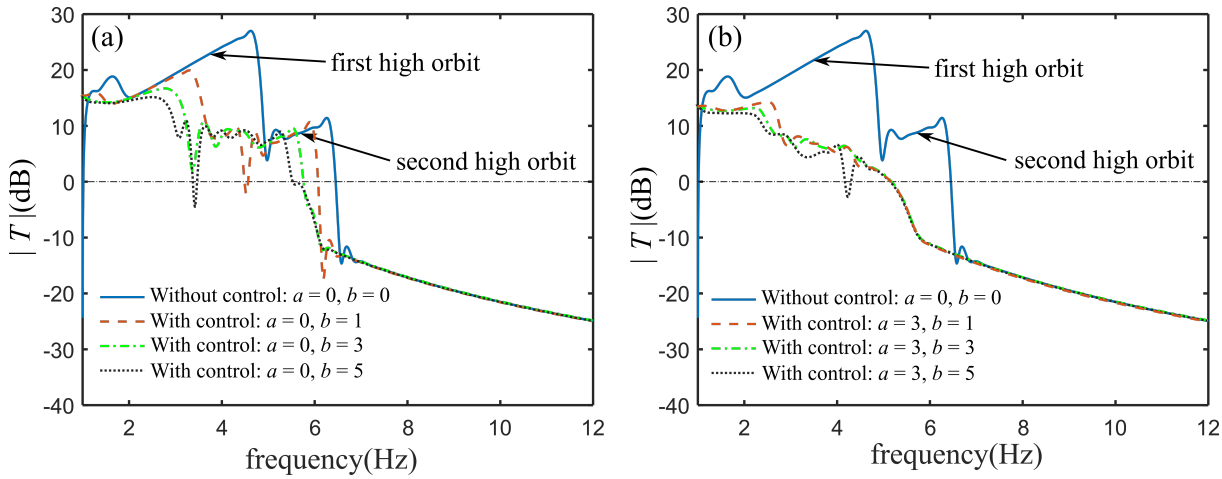

Fig. 12 Vibration transmissibility results of the EB-bistable actuator without and with active control subjected to different control weights for $A = 6$ m/s^2: (a) $a = 0,\ b = 1, 3, 5$ (b) $a = 3,\ b = 1, 3, 5$

7. Conclusions

This paper thoroughly investigates the active vibration isolation of the EB-bistable actuator subjected to the base excitation using the experimentally validated mathematical model. The control law combines the polynomial function of the payload absolute accelerations to significantly attenuate the vibration transmissibility from the base excitation to the actuator mover (supporting the payload). The results demonstrate that the active vibration isolation can not only attenuate the large-amplitude high-orbit vibration in the low frequency band, but also retain the vibration isolation performance in the high frequency band. The input-to-state stability of the control law for the non-negative control weights is proved, and the active vibration isolation is shown to be effective for different excitation strengths. Results of an investigated case have shown that, the maximum vibration transmissibility can be attenuated by over 90%. The lower bound of the effective vibration isolation bandwidth is reduced by 19.69%. The EB-bistable actuator without control may exhibit different types of dynamic behaviors for different initial conditions due to the implemented strong nonlinearity. However, the actuator with control can still demonstrate the effective vibration isolation for the initial condition variation. The parametric studies have shown that the higher the control weight, the better the vibration isolation. The linear-term control weight affects the active vibration isolation more significantly than the cubic-term control weight.

Acknowledgments

This work was supported by National Natural Science Foundation of China (Grant No.: 11802097).

References

[1] J. Awrejcewicz, D. Lewandowski, P. Olejnik, Dynamics of Mechatronics Systems: Modeling, Simulation, Control, Optimization and Experimental Investigations, World Scientific, 2016.

[2] J. Gajek, J. Awrejcewicz, Mathematical models and nonlinear dynamics of a linear electromagnetic motor, Nonlinear Dynamics, 94 (2018) 377-396.

[3] I. Maciejewski, M. Zlobinski, T. Krzyzynski, S. Glowinski, Vibration control of an active horizontal seat suspension with a permanent magnet synchronous motor, Journal of Sound and Vibration, 488 (2020).

[4] B. Yan, H.Y. Ma, W.G. Zheng, B. Jian, K. Wang, C.Y. Wu, Nonlinear Electromagnetic Shunt Damping for Nonlinear Vibration Isolators, Ieee-Asme Transactions on Mechatronics, 24 (2019) 1851-1860.

[5] R.K. Vashisht, Q.J. Peng, Fractional Calculus-Based Energy Efficient Active Chatter Control of Milling Process Using Small Size Electromagnetic Actuators, Journal of Vibration and Acoustics-Transactions of the Asme, 143 (2021).

[6] G.B. Gallego, L. Rossini, E. Onillon, T. Achtnich, C. Zwyssig, R. Seiler, D.M. Araujo, Y. Perriard, On-line micro-vibration measurement method for Lorentz-type magnetic-bearing space actuators, Mechatronics, 64 (2019).

[7] A.R. Tavakolpour-Saleh, M.A. Haddad, A fuzzy robust control scheme for vibration suppression of a nonlinear electromagnetic-actuated flexible system, Mechanical Systems and Signal Processing, 86 (2017) 86-107.

[8] N.A. Mansour, B. Shin, B. Ryu, Y. Kim, Development of a Novel Miniaturized Electromagnetic Actuator for a Modular Serial Manipulator, Actuators, 10 (2021).
[9] K. Song, S. Kim, Y. Cha, Soft electromagnetic actuator for assembly robots, Smart Materials and Structures, 29 (2020).
[10] D. Thanh Nho, P. Hung, N. Thuc-Quyen, Y. Visell, Miniature Soft Electromagnetic Actuators for Robotic Applications, Advanced Functional Materials, 28 (2018).
[11] K. Yang, R.L. Harne, K.W. Wang, H. Huang, Dynamic stabilization of a bistable suspension system attached to a flexible host structure for operational safety enhancement, Journal of Sound and Vibration, 333 (2014) 6651-6661.
[12] M. Derakhshani, N. Momenzadeh, T.A. Berfield, Analytical and experimental study of a clamped-clamped, bistable buckled beam low-frequency PVDF vibration energy harvester, Journal of Sound and Vibration, 497 (2021).
[13] J. Wang, L. Geng, K. Yang, L. Zhao, F. Wang, D. Yurchenko, Dynamics of the double-beam piezo-magneto-elastic nonlinear wind energy harvester exhibiting galloping-based vibration, Nonlinear Dynamics, 100 (2020) 1963-1983.
[14] K. Yang, F. Fei, H. An, Investigation of coupled lever-bistable nonlinear energy harvesters for enhancement of inter-well dynamic response, Nonlinear Dynamics, 96 (2019) 2369-2392.
[15] B. Yan, H. Ma, L. Zhang, W. Zheng, K. Wang, C. Wu, A bistable vibration isolator with nonlinear electromagnetic shunt damping, Mechanical Systems and Signal Processing, 136 (2020).
[16] Z. Zhang, X. Ni, H. Wu, M. Sun, G. Bao, H. Wu, S. Jiang, Pneumatically Actuated Soft Gripper with Bistable Structures, Soft Robotics, (2021).
[17] R. Addo-Akoto, J.-H. Han, Bidirectional actuation of buckled bistable beam using twisted string actuator, Journal of Intelligent Material Systems and Structures, 30 (2019) 506-516.
[18] H. Fang, K.W. Wang, Piezoelectric vibration-driven locomotion systems - Exploiting resonance and bistable dynamics, Journal of Sound and Vibration, 391 (2017) 153-169.
[19] A. Crivaro, R. Sheridan, M. Frecker, T.W. Simpson, P. Von Lockette, Bistable compliant mechanism using magneto active elastomer actuation, Journal of Intelligent Material Systems and Structures, 27 (2016) 2049-2061.
[20] R.L. Harne, K.W. Wang, Dipteran wing motor-inspired flapping flight versatility and effectiveness enhancement, Journal of the Royal Society Interface, 12 (2015).
[21] J.Z. Xuefeng Li, Renfu Li, Lu Dai, Wei Wang, Kai Yang,, Dynamic responses of a two-degree-of-freedom bistable electromagnetic energy harvester under filtered band-limited stochastic excitation, Journal of Sound and Vibration, 511 (2021).
[22] N. Yu, H. Ma, C. Wu, G. Yu, B. Yan, Modeling and experimental investigation of a novel bistable two-degree-of-freedom electromagnetic energy harvester, Mechanical Systems and Signal Processing, 156 (2021).
[23] K. Yang, Q. Zhou, Robust optimization of a dual-stage bistable nonlinear vibration energy harvester considering parametric uncertainties, Smart Materials and Structures, 28 (2019).
[24] J. Zhang, K. Yang, R. Li, A bistable nonlinear electromagnetic actuator with elastic boundary for actuation performance improvement, Nonlinear Dynamics, 100 (2020) 3575-3596.
[25] J. Zhang, X. Li, R. Li, L. Dai, W. Wang, K. Yang, Internal resonance of a two-degree-of-freedom tuned bistable electromagnetic actuator, Chaos Solitons & Fractals, 143 (2021).
[26] J. Zhang, X. Li, X. Feng, R. Li, L. Dai, K. Yang, A novel electromagnetic bistable vibration energy harvester with an elastic boundary: Numerical and experimental study, Mechanical Systems and Signal

Processing, 160 (2021).
[27] W. Chi, S.J. Ma, J.Q. Sun, A hybrid multi-degree-of-freedom vibration isolation platform for spacecrafts by the linear active disturbance rejection control, Applied Mathematics and Mechanics-English Edition, 41 (2020) 805-818.
[28] F. Zhang, S. Shao, Z. Tian, M. Xu, S. Xie, Active-passive hybrid vibration isolation with magnetic negative stiffness isolator based on Maxwell normal stress, Mechanical Systems and Signal Processing, 123 (2019) 244-263.
[29] M. Bednarek, D. Lewandowski, K. Polczyński, J. Awrejcewicz, On the active damping of vibrations using electromagnetic spring, Mechanics Based Design of Structures and Machines, (2020) 1-14.
[30] K. Polczyński, A. Wijata, J. Awrejcewicz, G. Wasilewski, Numerical and experimental study of dynamics of two pendulums under a magnetic field, Proceedings of the Institution of Mechanical Engineers, Part I: Journal of Systems and Control Engineering, 233 (2019) 441-453.
[31] A. Wijata, K. Polczyński, J. Awrejcewicz, Theoretical and numerical analysis of regular one-side oscillations in a single pendulum system driven by a magnetic field, Mechanical Systems and Signal Processing, 150 (2021) 107229.
[32] K. Polczyński, S. Skurativskyi, M. Bednarek, J. Awrejcewicz, Nonlinear oscillations of coupled pendulums subjected to an external magnetic stimulus, Mechanical Systems and Signal Processing, 154 (2021) 107560.
[33] J. Awrejcewicz, G. Kudra, G. Wasilewski, Experimental and numerical investigation of chaotic regions in the triple physical pendulum, Nonlinear Dynamics, 50 (2007) 755-766.
[34] J. Awrejcewicz, B. Supeł, C.-H. Lamarque, G. Kudra, G. Wasilewski, P. Olejnik, Numerical and experimental study of regular and chaotic motion of triple physical pendulum, International Journal of Bifurcation and Chaos, 18 (2008) 2883-2915.
[35] E.D. Sontag, Y. Wang, On characterizations of the input-to-state stability property, Systems & Control Letters, 24 (1995) 351-359.